

Flexibility aggregation via set projection for distribution grids with multiple interconnections

1st Maísa Beraldo Bandeira
 ie3 - Institute of Energy Systems,
 Energy Efficiency and Energy Economics
 TU Dortmund University
 Dortmund, Germany
 maisa.bandeira@tu-dortmund.de

2nd Alexander Engelmann
 logarithmo GmbH & Co. KG
 Dortmund, Germany
 alexander.engelmann@ieee.org

3rd Timm Faulwasser
 Institute of Control Systems
 Hamburg University of Technology
 Hamburg, Germany
 timm.faulwasser@ieee.org

Abstract—With the increasing number of flexible energy devices in distribution grids, coordination between Transmission System Operators (TSOs) and Distribution System Operators (DSOs) becomes critical for optimal system operation. One form of coordination is to solve the overall system operation problem in a hierarchical way, computing Feasible Operational Regions (FORs) for the interconnection between TSO/DSO. Most methods for computing FORs rely on the assumption of only one interconnection point between TSO and DSOs, which is often violated in practice. In this work, we propose a method for computing FORs in distribution grids with multiple interconnection points to the transmission grid. We test our method in a grid with two interconnecting points and analyze the properties of the resulting high-dimensional FOR from a power systems perspective.

Index Terms—Feasible Operational Region, Flexibility aggregation, Multiple Interconnections, TSO-DSO coordination

I. INTRODUCTION

Renewable energy sources and the electrification of the heating and mobility sectors offer large amounts of flexibility, which is a crucial lever for a cost-effective future system operation. As many of the corresponding devices are located in distribution grids, they play an increasingly active role in system operation. This raises the question of how to efficiently coordinate TSOs and DSOs. Controlling a large number of flexible devices directly at the TSO level is not desirable for many reasons, such as complexity and confidentiality.

Flexibility aggregation has been proposed for reducing complexity and simplifying information exchange. The approach relies on solving the centralized optimization problem in a hierarchical fashion. The first step is to compute Feasible Operational Regions (FORs) at the interconnection points between the Transmission System Operator (TSO) and Distributed System Operators (DSOs). A FOR is defined as the set of values for the coupling variables, usually active and reactive power, which can be achieved at the interconnection without violating the physical constraints of the distribution grid [1]. The TSO uses the FOR in its own optimization problem, leveraging the flexibility of DERs without causing congestion for the DSO.

Several methods for computing the FOR, also referred to as flexibility aggregation, have been proposed in the literature [2]. Most of these approaches rely on sampling the feasible region

and subsequently computing the convex hull of the resulting points. Different sampling strategies can be employed—for instance, Monte Carlo methods [3], which, however, require a large number of samples. Alternatively, the samples can be determined more systematically by solving an optimal power flow problem to obtain the extreme operating points of the FOR, i.e., the maximum and minimum active and reactive power exchanges at the interconnection [4, 5]. These methods perform well for two-dimensional FORs, i.e. for simple PQ-charts. In [6], swarm optimization is used to compute multiple samples that explicitly account for the voltage dependency.

In practice, the interconnection point between grid operators is not always unique. In Germany, for example, it is quite common that the TSO and DSO have at least two interconnection points. There are limited works in the literature that address the problem of computing the FOR for more than one interconnection point, since it is not trivial to extend the sampling methods presented above to that scenario. The challenge arises from the mutual dependence between the powers at the different interconnections and the physical distance between the buses to which they are connected in the transmission grid, which influences the voltages.

The work in [7] extends the method for a grid with two interconnecting points. It computes two independent FORs by sampling them individually. The coupling between the two interconnection points is considered by deriving a data-based equivalent grid for the transmission grid, but the intrinsic dependency of the flexibility available at each interconnection is neglected. Alternatively, the work in [8] computes an equivalent grid for the distribution grid, rather than a FOR, communicating to the TSO more information than just the feasible values for the coupling variables. However, the authors highlight the importance of the voltage magnitude and angle dependency at the coupling points.

Furthermore, in [9], the interdependence between the FORs is highlighted. Building on this, [10] explicitly considers the relationship between the two FORs. They first compute the FOR for one interconnection using an optimization-based sampling procedure. The resulting feasible area is then discretized into a grid. For each grid cell—representing a specific range of power exchange at the first interconnection—the method

computes a corresponding FOR for the second interconnection, again via sampling. The approach yields a set of pairs of FORs for the two interconnections, which is difficult to incorporate directly into the TSO optimization problem.

Recently, set projection has been used for the computation of the FOR [11, 12]. The method has been extended to multi-dimensional FORs, which include time-dependent elements [13]. In [14] set projection was used for the coordination of transmission grids with multiple connections, using a linearized version of the grid that takes into consideration only active power.

However, despite its practical relevance, and to the best of the authors' knowledge, the computation of high-dimensional FORs for distribution grids with multiple interconnections has not been addressed before. Building on our earlier work [12], we extend the set projection approach to this setting, enabling the computation of multidimensional FORs that capture all the couplings between interconnection variables. Using a linearized power flow formulation that preserves voltage and reactive power information, the resulting polyhedral FOR can be readily communicated to the TSO as a compact set of inequality constraints. The approach is demonstrated and analyzed for a distribution grid with two interconnection points.

The paper is organized as follows: first, we define our problem and explain our approach for flexibility aggregation in Section II. In Section III, we present our case study and results. Lastly, Section IV summarizes our findings and outlines possible future research directions.

II. PROBLEM SET-UP

We assume the power system to be tree-structured, with the distribution grids having no connections to one another. We define the multi-voltage level power system as a graph $G^e = (\mathcal{N}, \mathcal{B})$, where each node $k \in \mathcal{N}$ is a bus and the edges $(k, l) \in \mathcal{B}$ represent the branches that connect the buses, e.g., transmission lines or transformers.

We consider by $i \in \mathcal{S} = \{1, \dots, |\mathcal{S}|\}$, where $i = 1$ refers to the TSO and the index set $\mathcal{D} \doteq \mathcal{S} \setminus \{1\}$ refers to the DSOs. Furthermore, we decompose the set of buses \mathcal{N} into a set with the TSO buses \mathcal{N}_1 and into $|\mathcal{D}|$ bus sets for the DSOs $\mathcal{N}_i, i \in \mathcal{D}$, for all DSOs. Similarly, we split the set of branches \mathcal{B} into $\{\mathcal{B}_i\}_{i \in \mathcal{S}}$ such that all branches connecting nodes in \mathcal{N}_i belong to \mathcal{B}_i . We assign the branches connecting TSO and DSO grids $\mathcal{B}_i^c \subseteq \mathcal{B}_i$ to the DSOs. We denote the buses at the TSO level connected to a branch between TSO and DSO i as $\mathcal{N}_i^c \subseteq \mathcal{N}$. Details of the formulation can be found in [15].

The corresponding OPF problem reads

$$\min_{\{y_i\}_{i \in \mathcal{S}}, \{z_i\}_{i \in \mathcal{D}}} f_1(y_1) + \sum_{i \in \mathcal{D}} f_i(y_i, z_i) \quad (1a)$$

$$\text{subject to } (y_i, z_i) \in \mathcal{X}_i \text{ for all } i \in \mathcal{D} \quad (1b)$$

$$(y_1, z_2, \dots, z_{|\mathcal{S}|}) \in \mathcal{X}_1, \quad (1c)$$

where for each subsystem i , we denote the local decision variables as $y_i \subseteq x_i$ and the coupling variables as $z_i \subseteq x_i$,¹ i.e., variables that appear both in the TSO and the DSO problem, so that $x_i = (y_i, z_i)$. Furthermore, \mathcal{X}_i are local constraint sets of DSOs or the TSO.

A. The constraint sets \mathcal{X}_i

The physical characteristics and limitations of each subgrid define the feasible sets \mathcal{X}_i of the subproblems. To utilize existing polyhedral set projection tools, we formulate these sets as a convex polyhedron. In [12], we compare different convex grid models, which lead to polyhedral constraint sets convenient for flexibility aggregation for grids with only one interconnection point. All models except the DC power flow formulation are limited to radial grids.

Since the DC model is too inaccurate for distribution grid analysis and the other approaches are limited to one interconnection, we employ a Taylor series linearization of the AC power flow equations using polar coordinates [16], which doesn't require the grid to be radial. In the instance used here, there is no representation for the current. However, the formulation can be extended to include current information [17].

Assume that we have a balanced grid and zero line-charging capacitances. The associated bus-admittance matrix $Y = G + jB \in \mathbb{C}^{|\mathcal{N}| \times |\mathcal{N}|}$ is defined as

$$[Y]_{k,l} = \begin{cases} \sum_{k \in \mathcal{N}} y_{k,l} & \text{if } k = l, \\ -y_{k,l}, & \text{if } k \neq l. \end{cases}$$

Here, $y_{k,l} = g_{k,l} + jb_{k,l} \in \mathbb{C}$ is the admittance of branch $(k, l) \in \mathcal{B}$, and $b_{k,l}$ and $g_{k,l}$ are its susceptance and conductance, respectively. Note that $y_{k,l} = 0$ if $(k, l) \notin \mathcal{B}$. The flow of active power and reactive power along branch $(k, l) \in \mathcal{B}$ is given by

$$p_{k,l} = v_k v_l (G_{k,l} \cos(\theta_{k,l}) + B_{k,l} \sin(\theta_{k,l})), \quad (2a)$$

$$q_{k,l} = v_k v_l (G_{k,l} \sin(\theta_{k,l}) - B_{k,l} \cos(\theta_{k,l})). \quad (2b)$$

Here, v_k is the voltage magnitude at node $k \in \mathcal{N}$ and $\theta_{k,l} \doteq \theta_k - \theta_l$ is the voltage angle difference between the two nodes $k, l \in \mathcal{N}$.

Using (2), the AC power flow equations for all buses $k \in \mathcal{N}$ read

$$p_k = \sum_{l \in \mathcal{N}} p_{k,l}, \quad q_k = \sum_{l \in \mathcal{N}} q_{k,l}, \quad (3)$$

where $p_k, q_k \in \mathbb{R}$ are the net active and reactive power injection at node $k \in \mathcal{N}$.

The active and reactive power at each bus is defined as

$$p_k = p_k^g - p_k^d, \quad (4)$$

$$q_k = q_k^g - q_k^d \quad (5)$$

¹We use the shorthand $y \subset x$, $y \in \mathbb{R}^n$, $x \in \mathbb{R}^m$, $n < m$ to express that y is composed of a subset of the components of x , i.e., there exists an index set $\mathcal{I} \subset \{1, \dots, m\}$ such that $y = [x_i]_{i \in \mathcal{I}}$, where $[\cdot]$ denotes the vertical concatenation.

for all $k \in \mathcal{N}$, where p_k^g and q_k^g represent the active/reactive power feed-in at node k and p_k^d and q_k^d the active/reactive power demand.

To derive a linearized approximation of the AC power flow equations, we define $(p_k^o, q_k^o, v_k^o, \theta_k^o)$ as the operating point. Let $P, Q \in \mathbb{R}^{|\mathcal{N}|}$ denote the vectors of active and reactive power injections, $[p_k]_{k \in \mathcal{N}}$ and $[q_k]_{k \in \mathcal{N}}$, respectively, and let $V, \theta \in \mathbb{R}^{|\mathcal{N}|}$ denote the vectors of voltage magnitudes and angles, $[v_k]_{k \in \mathcal{N}}$ and $[\theta_k]_{k \in \mathcal{N}}$.

Using a first-order Taylor expansion of (3) around the operating point (V^o, θ^o) , we obtain

$$\begin{bmatrix} P \\ Q \end{bmatrix} = \begin{bmatrix} P^o \\ Q^o \end{bmatrix} + J|_{(V^o, \theta^o)} \begin{bmatrix} \theta - \theta^o \\ V - V^o \end{bmatrix}, \quad (6)$$

where the Jacobian J is given by

$$J = \begin{bmatrix} \frac{\partial P}{\partial \theta} & \frac{\partial P}{\partial V} \\ \frac{\partial Q}{\partial \theta} & \frac{\partial Q}{\partial V} \end{bmatrix}. \quad (7)$$

The submatrices of J represent the sensitivities of active and reactive power injections with respect to voltage angles and magnitudes, as defined by the nonlinear AC power flow equations (2)–(3). Explicit expressions for the entries of J in polar coordinates can be found in [16, 18]. This linearized model provides a convex approximation of the feasible set, used to construct the polyhedral constraint sets \mathcal{X}_i .

Besides the power flow constraints, the active power generation must stay within lower and upper bounds. Let $\mathcal{G} \subseteq \mathcal{N}$ denote the set of generator buses, then

$$p_k^g \leq p_k^g \leq \bar{p}_k^g, \quad k \in \mathcal{G}. \quad (8)$$

For “flexible” renewable generators, i.e., generators which can alter their set points, we have $\underline{p}_k^g = 0$ and $\bar{p}_k = f_k^g$, where f_k^g represents the maximal power feed in given by irradiation/wind conditions. Moreover, the renewable generators $k \in \mathcal{G}$ can offer reactive power support q_k , constrained by the maximum apparent power \bar{s}_k and a power factor limit α . Thus, we consider affine constraints [19]

$$p_k^g \leq \bar{s}_k \cos(\alpha), \quad -p_k \leq \alpha q_k \leq p_k. \quad (9)$$

Additionally, we constrain the voltage magnitude at all buses to stay within bounds

$$\underline{v}_k \leq v_k \leq \bar{v}_k. \quad (10)$$

Finally, we constrain the active power flowing into the grid at the set of interconnecting branches $(k, l) \in \mathcal{B}_i^c$, so that both nodes are only importing power from the TSO.

$$p_{k,l} \geq 0. \quad (11)$$

The final constraint set for the individual DSO’s reads

$$\mathcal{X}_i \doteq \{x_i \in \mathbb{R}^{n_{x_i}} \mid (6)–(11) \text{ hold } \forall k \in \mathcal{N}_i, \text{ and } \forall (k, l) \in \mathcal{B}_i\}$$

where $x_i \doteq [p_k^g, q_k^g, p_k, q_k, v_k, \theta_k]_{k \in \mathcal{N}_i}, [p_{k,l}, q_{k,l}]_{(k,l) \in \mathcal{B}_i}^\top\}$ for all $i \in \mathcal{C}$. Analogously, \mathcal{X}_1 denotes the feasible set of the TSO, capturing the transmission-level power flow constraints and operational limits.

B. Flexibility aggregation via set projection

We can now define the coupling variable $z_i^\top \doteq [[p_{k,l}, q_{k,l}]_{(k,l) \in \mathcal{B}_i^c}, [v_k, \theta_k]_{k \in \mathcal{N}_i^c}]$. The importance of considering the voltage magnitude as a coupling variable has been demonstrated in [12]. There, the voltage angle at the interconnection is considered equal to zero and not a coupling variable. For the AC power flow equations, the active and reactive power on branch $(k, l) \in \mathcal{B}$ depends only on the voltage angle difference $(\theta_k - \theta_l)$. We have $p_{k,l}(v_k, v_l, \theta_k, \theta_l) = p_{k,l}(v_k, v_l, \theta_k + \bar{\theta}, \theta_l + \bar{\theta})$ for any $\bar{\theta} \in \mathbb{R}$, so setting $\theta_k = 0$ in \mathcal{X}_i does not alter the solution space. Here, no such simplification can be made. We must consider the angle difference between the interconnections, as shown in [8], but not their actual value. The difference is invariant w.r.t. a constant offset.

We propose to look at aggregation as equivalent to a set projection of the feasible set of the DSOs, \mathcal{X}_i , on the coupling variables z_i . The *set projection* of $\mathcal{X} \subseteq \mathcal{Y} \times \mathcal{Z}$ onto \mathcal{Z} is defined as [20]

$$\text{proj}_{\mathcal{Z}}(\mathcal{X}) \doteq \{z \in \mathcal{Z} \mid \exists y \in \mathcal{Y} \text{ with } (z, y) \in \mathcal{X}\} \subseteq \mathcal{Z}. \quad (12)$$

The above definition (12) can be interpreted as searching for all coupling variables to the TSO, z_i , for which there exist local variables y_i , i.e., admissible set-points of the local DERs, which satisfy all grid constraints. Hence, aggregation can be interpreted as computing the FOR

$$\mathcal{P}_i \doteq \text{proj}_{\mathcal{Z}_i} \mathcal{X}_i. \quad (13)$$

There are many advantages to computing the FOR using set projection. First, it is a flexible approach, since we can define the coupling variable depending on the task at hand, without altering the methodology or the framework. Additionally, if using polytope set projection, the resulting FOR can be expressed as the polytope $A_i z_i \leq b_i$. The DSO then only needs to communicate the matrices A_i, b_i to the TSO, which can then easily add the linear inequalities to its own optimization problem, without adding much complexity. Here, we focus on the flexibility aggregation of one distribution grid with multiple interconnections, i.e. the computation of the FOR \mathcal{P}_i .

III. SIMULATION

For the simulation, we employ the CIGRE Medium Voltage European Grid testbench [21], which represents a meshed distribution network with two transformers connecting to the high-voltage grid, as illustrated in Figure 1. Renewable generators are placed at nodes 6, 8, and 12, and their active power feed-in capacities are doubled relative to the original specification. Following the setup in the original benchmark, we first consider the case in which both interconnection points connect to the same high-voltage bus, i.e., node 1 = node 16.

A. Suitability of approximation

Firstly, we evaluate the suitability of the linearized formulation introduced in Section II for the purpose of flexibility aggregation in the meshed distribution grid. Specifically, we compare the resulting FOR with that obtained using an

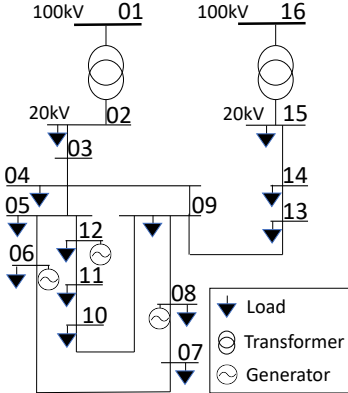


Fig. 1: CIGRE medium voltage European grid [21].

optimization-based sampling method based on the nonlinear AC power flow formulation introduced in the literature.

To this end, we compute samples $z_k^s = (p_{k,l}, q_{k,l})$ by solving multiple optimization problems of the form

$$z_k^t = \arg \min_{z_i, y_i} c_i^\top z_k \quad \text{subject to} \quad (y_i, z_i) \in \mathcal{X}_i^{AC}, \quad (14)$$

where we assume the voltage magnitude and angle reference

$$v_k = 1 \text{ p.u.}, \quad \theta_k = 0, \quad (15)$$

and define

$$\mathcal{X}_i^{AC} \doteq \left\{ x_i \in \mathbb{R}^{n_{x_i}} \mid (2)-(5), (8)-(11), \text{ and (15)} \right. \\ \left. \text{hold } \forall k \in \mathcal{N}_i, (k, l) \in \mathcal{B}_i \right\}.$$

Different boundary points of the FOR are obtained by varying the cost vector $c_l \in -1, 0, 1^{n_z}$ to explore the extreme points [4, 5]. To refine the sampling, the resulting region is discretized, and one variable component is fixed for each grid point before re-solving (14). A detailed description of this process is provided in [22]. The resulting FOR is defined as

$$\mathcal{F}_i = \text{conv}(\{z_k^t\}_{t \in \mathcal{T}}),$$

where \mathcal{T} denotes the set of all sample indices and $\text{conv}(\mathcal{W})$ denotes the convex hull over a set of points \mathcal{W} .

Subsequently, we compute the linearized FOR $\tilde{\mathcal{P}}_i$ as described in Section II,

$$\tilde{\mathcal{P}}_i = \text{proj}_{z_i}(\tilde{\mathcal{X}}_i)$$

with $z_i = [p_{k,l}, q_{k,l}]^\top$ and the extended constraint set

$$\tilde{\mathcal{X}}_i \doteq \left\{ x_i \in \mathcal{X}_i \mid (15) \text{ holds} \right\}.$$

The operating point is chosen as the solution of

$$(x_i^\circ, z_i^\circ) = \arg \min_{x_i, z_i} \sum_{k \in \mathcal{G}} \left[-c_1(p_k^g)^2 + c_2(q_k^g)^2 \right] \quad (16)$$

$$\text{subject to } (x_i, z_i) \in \mathcal{X}_i^{AC}. \quad (17)$$

corresponding to the case that minimizes the power curtailment of renewable generators. The resulting regions are depicted in Figure 2. The linearized formulation approximates the FOR

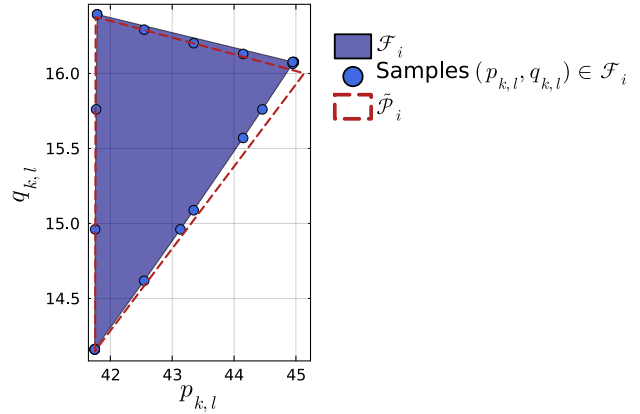


Fig. 2: Comparison of FORs obtained with AC-OPF sampling and the proposed linearized set projection method for a single interconnection point.

obtained with the AC model closely, although it includes certain infeasible points that may lead to infeasibility in the coupled optimization problem [22].

B. Flexibility aggregation via set projection

Now, with a reasonably good approximation for the one interconnection bus case, we portray the interconnection buses as in Figure 1, as two independent buses, $k = 1$ and $k = 16$, each connected to one of the different transformers. We then extend the coupling variables for the multi-interconnections case as the 8-dimensional vector $z_i \doteq [p_{1,2}, q_{1,2}, v_1, \theta_1, p_{16,15}, q_{16,15}, v_{16}, \theta_{16}]$. Since in this case we have only two interconnections, and as explained in Section II the difference between the angles is what matters, we set $\theta_0 = 0$ and use $\theta_1 - \theta_{16}$ as the coupling variable, reducing the coupling vector to 7 dimensions.

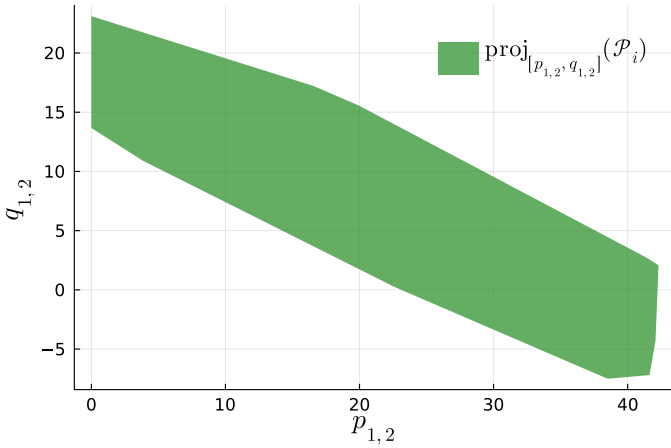
By projecting the full constraint set \mathcal{X}_i into the coupling variable z_i , we obtain a FOR, which is a 7-dimensional polyhedron, representing the flexibility available at each interconnection as well as the dependent relationship between the variables.

C. Results discussion

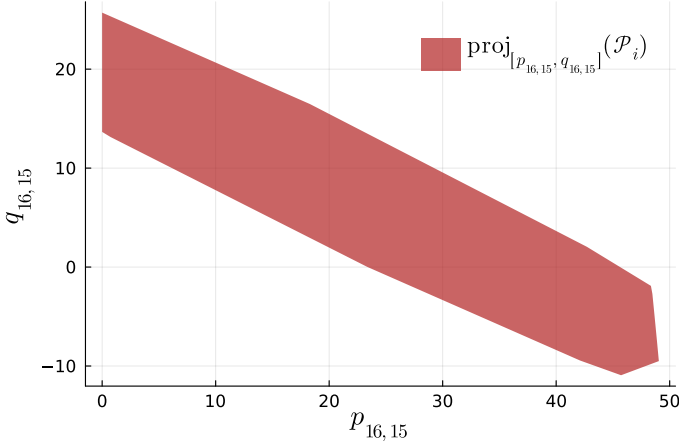
To interpret the abstract results in a more tangible way, we illustrate the relationship between pairs of variables, using the set projection, of the 7D-polyhedron into the desired two variables.

First, we analyze the aggregated active and reactive power at the individual interconnections. As shown in Figure 3, the available maximum power at each interconnection differs due to the location of the assets. It is important to note that these results should not be considered in isolation—neither relative to each other nor to the remaining variables—as all are interconnected. In other words, these charts cannot be interpreted independently.

To better illustrate this point, we analyze the dependency of the active power in one interconnection on the active power in the second interconnection. More specifically, Figure 4



(a) Active and reactive power at interconnection on line (1, 2)



(b) Active and reactive power at interconnection on line (16, 15)

Fig. 3: Projected views for active and reactive power of the 7D-FOR for the case with two interconnection points.

illustrates a negative dependency between the two active powers: as the active power flowing into the distribution grid increases at one interconnection, it decreases at the other. This indicates that the power demand can be met through both interconnections, such that a higher export on one side reduces the power supplied from the other. The interior of the FOR reflects the inherent flexibilities within the distribution grid. The dashed line represents the area where the renewable generators' power feed-in is not increased, illustrating the reduced flexibility within the grid.

Next, we compare the active and reactive power requirements to the single-interconnection case, as shown in Figure 2. To this end, we define the aggregated variables

$$p_{\text{sum}} = p_{1,2} + p_{16,15}, \quad q_{\text{sum}} = q_{1,2} + q_{16,15},$$

and compute the corresponding FOR via projection as

$$\mathcal{P}'_i = \text{proj}_{[p_{\text{sum}}, q_{\text{sum}}, v_1, v_{16}, \theta_1 - \theta_{16}]}(\mathcal{X}_i),$$

where \mathcal{X}_i is the extended constraint set including the voltage and power flow constraints at both interconnection buses.

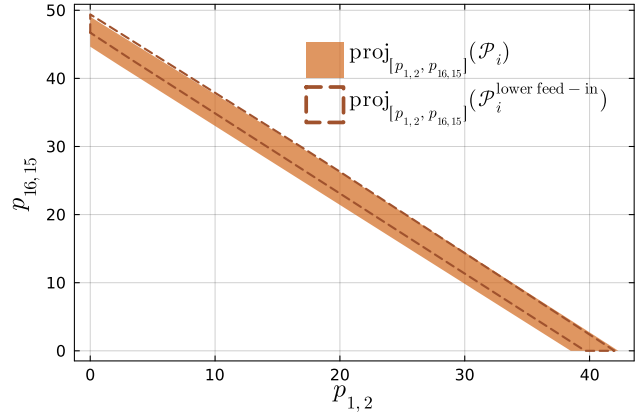


Fig. 4: Visualization of the relationship between active power flows $p_{1,2}$ and $p_{16,15}$ based on the 7D-FOR projection.

Since the grid topology now includes two independent interconnections, the FOR depends not only on the total power exchange but also on the individual voltage magnitudes v_1 , v_{16} and the relative voltage angle $\theta_1 - \theta_{16}$. Therefore, we consider three distinct case setups to isolate the effects of these additional degrees of freedom:

TABLE I: Overview of the considered cases and corresponding constraints on the interconnection buses.

Case	Voltage magnitudes	Angle difference
1	v_1, v_{16} free	$\theta_1 - \theta_{16}$ free
2	v_1, v_{16} free	$\theta_1 - \theta_{16} = 0$
3	$v_1 = v_{16} = 1$ p.u.	$\theta_1 - \theta_{16} = 0$

In Case 1, all interconnection variables are free, resulting in the largest FOR. Case 2 constrains the angle difference, effectively reducing the dimensionality of the feasible region and leading to a smaller FOR, shown in Figure 5 in orange. Finally, Case 3 fixes both voltage magnitudes and the angle difference, producing a region comparable to the single-interconnection scenario (Figure 2). These comparisons illustrate how the additional degrees of freedom in multi-interconnection grids influence the aggregated flexibility and highlight the importance of including both voltage and angle variations in the FOR computation.

These observations are directly explainable from a power systems perspective. In Case 3, where the voltage angles and magnitudes are fixed, we essentially recover the scenario in which both interconnections are connected to the same bus, yielding a FOR identical to that in Figure 2. In the other cases, the voltage angles and magnitudes are allowed to vary, and in the extreme case where they are completely free (Case 1).

From a TSO perspective, this behavior is intuitive: multiple interconnections enable the distribution grid to be used for both flexibility provision and power transfer between buses. It is important to note, however, that in a real transmission system, the voltage angles and magnitudes at the interconnection buses are not entirely free; they are influenced by the

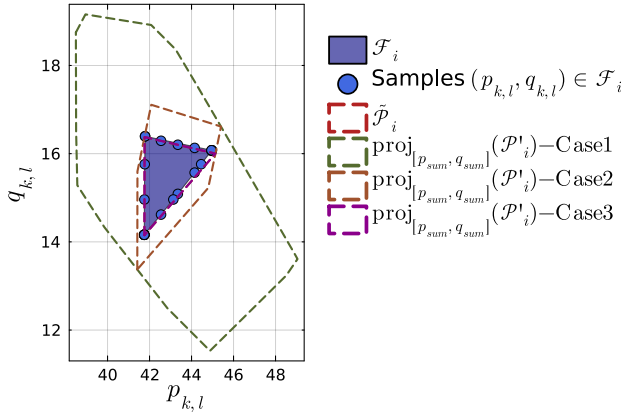


Fig. 5: Total active and reactive power requirements for the three cases of the two-interconnection scenario, compared to the single-interconnection case.

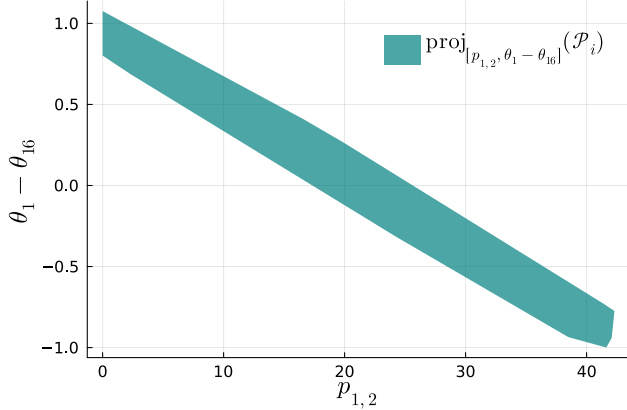


Fig. 6: Visualization of the relationship between active power $p_{1,2}$ and the voltage angle difference $\theta_1 - \theta_{16}$ based on the 7D-FOR projection.

connected TSO grid, its electrical parameters, and the setpoints of the deployed equipment.

The dependency between the active power at one interconnection and the voltage angle difference can be visualized by projecting our 7-dimensional FOR onto the variables $p_{1,2}$ and $\theta_1 - \theta_{16}$, as shown in Figure 6. The projection highlights how variations in the angle difference directly influence the feasible range of active power that can be drawn from the distribution grid at this interconnection. A similar relationship is observed for the other interconnection, $p_{16,15}$, reflecting the inherent coupling between the interconnections in the network. These projections provide an intuitive view of how the flexibility of the distribution grid is constrained by both network topology and voltage conditions.

This dependency may also help explain the differences observed in the computed regions in [7, 8]. In that work, the flexibility areas obtained using an equivalent circuit for the transmission or distribution grid are smaller than those computed for the distribution grid in isolation. This can be attributed to the natural restriction of the voltage differences

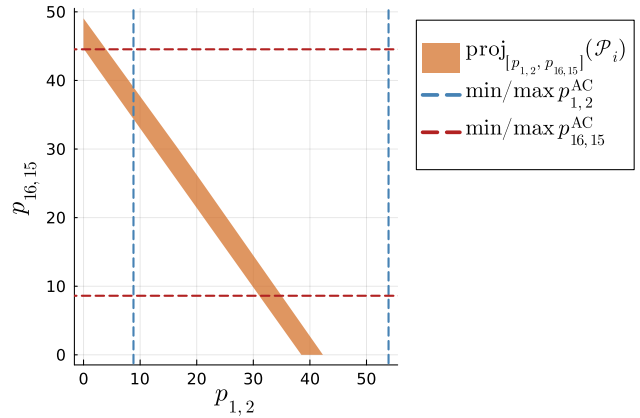


Fig. 7: Projection of the 7D-FOR onto active powers $p_{1,2}$ and $p_{16,15}$ for the two-interconnection scenario, compared to AC-OPF extreme values sampling results for the same case.

imposed by the physical properties of the transmission grid. In contrast, our aggregated 7D-FOR explicitly accounts for the voltage magnitude and angle coupling. As a result, when the TSO receives the 7D-FOR, it will inherently operate within the subset of the region that is feasible according to its own grid constraints, making an equivalent circuit representation unnecessary.

Lastly, we examine the potential modeling inaccuracies of the chosen power flow formulation due to linearization and its implications on the high-dimensional FOR. Although we cannot easily compute the 7D-FOR with the AC power flow, we can solve the optimization problem for the maximum values to get an idea of the difference. By treating multiple variables as coupling variables, the resulting operating points may lie farther from the linearization points, which inevitably increases potential linearization errors near the boundary of the high-dimensional FOR, as illustrated in Figure 7. The actual impact of these errors on system operation, however, depends on the TSO's decisions: points near the FOR boundary may introduce inaccuracies, whereas points closer to the linearization point are expected to be less critical.

IV. CONCLUSION AND OUTLOOK

We have presented a flexibility aggregation scheme for distribution grids with multiple interconnections. We have extended works based on set projections to be applied to grids with two or more interconnections. The resulting multidimensional FOR helps to gain insight into the relationship between the physical variables at both interconnections and can be easily communicated to the upper grid as a polytope. In future work, we will look into different linear formulations for meshed grids that can be used for set projection and model the behavior of the grid outside of the operational point better. A further aspect is to make the projection step itself more efficient, e.g., by using inner approximations of the FOR, which are easier to project.

REFERENCES

- [1] D. Mayorga Gonzalez, J. Hachenberger, J. Hinker, F. Rewald, U. Häger, C. Rehtanz, and J. Myrzik, "Determination of the Time-Dependent Flexibility of Active Distribution Networks to Control Their TSO-DSO Interconnection Power Flow," in *Power Systems Computation Conference (PSCC)*, 2018, pp. 1–8.
- [2] M. Sarstedt, L. Kluß, J. Gerster, T. Meldau, and L. Hofmann, "Survey and Comparison of Optimization-Based Aggregation Methods for the Determination of the Flexibility Potentials at Vertical System Interconnections," *Energies*, vol. 14, no. 3, p. 687, 2021.
- [3] D. Mayorga Gonzalez, J. Hachenberger, J. Hinker, F. Rewald, U. Häger, C. Rehtanz, and J. Myrzik, "Determination of the Time-Dependent Flexibility of Active Distribution Networks to Control Their TSO-DSO Interconnection Power Flow," in *2018 Power Systems Computation Conference (PSCC)*, 2018, pp. 1–8.
- [4] J. Silva, J. Sumaili, R. J. Bessa, L. Seca, M. A. Matos, V. Miranda, M. Caujolle, B. Goncer, and M. Sebastian-Viana, "Estimating the active and reactive power flexibility area at the TSO-DSO interface," *IEEE Transactions on Power Systems*, vol. 33, no. 5, pp. 4741–4750, 2018.
- [5] F. Capitanescu, "TSO-DSO interaction: Active distribution network power chart for TSO ancillary services provision," *Electric Power Systems Research*, vol. 163, pp. 226–230, 2018.
- [6] M. Sarstedt, L. Kluß, M. Dokus, L. Hofmann, and J. Gerster, "Simulation of Hierarchical Multi-Level Grid Control Strategies," in *2020 International Conference on Smart Grids and Energy Systems (SGES)*, Perth, Australia: IEEE, 2020, pp. 175–180.
- [7] J. Silva, J. Sumaili, B. Silva, L. Carvalho, F. Retorta, M. Staudt, and V. Miranda, "A Data-Driven Approach to Estimate the Flexibility Maps in Multiple TSO-DSO Connections," *IEEE Transactions on Power Systems*, vol. 38, no. 2, pp. 1908–1919, 2023.
- [8] L. Stark and L. Hofmann, "Novel Approach for Flexibility Aggregation at Multiple Vertical TSO-DSO Interconnections," in *Transformation Der Stromversorgung – Netzregelung Und Systemführung: 15. ETG/GMA-Fachtagung, Netzregelung Und Systemführung*, 2024, pp. 18–24.
- [9] N. Majumdar, M. Sarstedt, and L. Hofmann, *Distribution grid power flexibility aggregation at multiple interconnections between the high and extra high voltage grid levels*, 2023. eprint: 2303.01107.
- [10] L. Stark, M. Sarstedt, and L. Hofmann, "Determination of Interdependent Feasible Operation Regions at Multiple TSO-DSO Interconnections," in *2023 IEEE PES Innovative Smart Grid Technologies Europe (ISGT EUROPE)*, 2023, pp. 1–6.
- [11] Z. Tan, Z. Yan, H. Zhong, and Q. Xia, "Non-Iterative Solution for Coordinated Optimal Dispatch via Equivalent Projection—Part I: Theory," *IEEE Transactions on Power Systems*, vol. 39, no. 1, pp. 890–898, 2024.
- [12] M. Beraldo Bandeira, T. Faulwasser, and A. Engelmann, "An ADP Framework for Flexibility and Cost Aggregation: Guarantees and Open Problems," *Electric Power Systems Research*, vol. 234, p. 110818, 2024.
- [13] Y. Wang, H. Zhong, and G. Ruan, "A Projection-Based Approach for Distributed Energy Resources Aggregation," in *2023 IEEE PES Innovative Smart Grid Technologies Europe (ISGT EUROPE)*, 2023, pp. 1–5.
- [14] C. Lyu, L. He, Z. Tan, Y. Lin, X. Luo, and Z. Yan, "Feasible Set Projection Method for Calculating Multi-Line-Coupled ATC," in *2023 3rd Power System and Green Energy Conference (PSGEC)*, 2023, pp. 791–797.
- [15] M. B. Bandeira, A. Engelmann, and T. Faulwasser, *Complexity Reduction for TSO-DSO Coordination: Flexibility Aggregation vs. Distributed Optimization*, 2025. arXiv: 2509.10595 [eess].
- [16] D. K. Molzahn and I. A. Hiskens, "A Survey of Relaxations and Approximations of the Power Flow Equations," *Foundations and Trends® in Electric Energy Systems*, vol. 4, no. 1-2, pp. 1–221, 2019.
- [17] T. Leveringhaus and L. Hofmann, "Comparison of methods for state prediction: Power Flow Decomposition (PFD), AC Power Transfer Distribution factors (AC-PTDFs), and Power Transfer Distribution factors (PTDFs)," in *2014 IEEE PES Asia-Pacific Power and Energy Engineering Conference (APPEEC)*, 2014, pp. 1–6.
- [18] R. D. Zimmerman, "AC Power Flows, Generalized OPF Costs and their Derivatives using Complex Matrix Notation," *Matpower*, Tech. Rep., 2010.
- [19] D. A. Contreras and K. Rudion, "Time-Based Aggregation of Flexibility at the TSO-DSO Interconnection Point," in *IEEE Power & Energy Society General Meeting (PESGM)*, 2019, pp. 1–5.
- [20] S. Rakovic, E. Kerrigan, D. Mayne, and J. Lygeros, "Reachability analysis of discrete-time systems with disturbances," *IEEE Transactions on Automatic Control*, vol. 51, no. 4, pp. 546–561, 2006.
- [21] Conseil international des grands réseaux électriques, Ed., *Benchmark Systems for Network Integration of Renewable and Distributed Energy Resources*. Paris: CIGRÉ, 2014.
- [22] A. Engelmann, M. B. Bandeira, and T. Faulwasser, "Approximate Dynamic Programming With Feasibility Guarantees," *IEEE Transactions on Control of Network Systems*, pp. 1565–1576, 2025.